Theory of superplasticity in polycrystalline materials: Stress-induced structural instabilities of grain boundaries

Miguel Lagos*
Departamento de Física, Facultad de Ciencias, Universidad de Chile, Casilla 653, Santiago, Chile
(Received 11 August 2004; revised manuscript received 17 March 2005; published 30 June 2005)

A fine mechanical analysis of a polycrystalline material subjected to large stresses must distinguish between intergranular and crystalline matter because they have different mechanical properties. Homogeneity is an illusion at the grain level. It is shown that a grain boundary under the action of a strong enough in-plane shear stress becomes unstable, buckling into periodic trenches or a corrugated profile. The former should always occur; the latter demands the existence of steps, intersecting hard particles or triple junctions. Strongly varying stress fields, spontaneously induced to preserve mechanical equilibrium at the grain scale, cause intergranular matter to begin to release and capture vacancies in alternate sectors. The subsequent active lattice diffusion near the buckled boundary causes adjacent crystallites to slide. The effect is translated into the macroscopic scale to derive a closed-form constitutive equation relating stress, strain rate, temperature, grain size, and grain boundary thickness, without undetermined parameters. The agreement with available experimental data on the superplastic deformation of alloys, over the whole range of strain rates and temperatures, is remarkable. Applications to Al-8090 SPF, Al-7475, and Ti-6Al-4V are shown. The degradation of superplastic properties at high strain rates or temperatures is explained.

DOI: 10.1103/PhysRevB.71.224117 PACS number(s): 62.20.Fe, 46.32.+x, 61.72.Mm, 61.72.Ji

I. INTRODUCTION

High-strength superplastic materials offer important and attractive engineering applications because they exhibit outstanding mechanical properties and allow for special fabrication techniques. Most uses occur in the aerospace industry, which currently applies superplastic aluminum and titanium alloys for the production of airplane structural components[1] and engine parts. Superplastic forming combined with diffusion bonding is a standard technique for producing the hollow wide chord blades of large turbofan engines. In the race for more efficient aeroengines, lighter TiAl-based alloys are promising candidates to replace the nickel-based superalloys in turbine blades and combustion chambers. However, besides these large technical advances, the atomic mechanism which produces superplastic behavior is currently under discussion and remains as an open solid-state physical problem.

Surprisingly, superplastic flow takes place in a relatively narrow range of temperature, which is ordinarily far below the melting point. The strain rate also has a finite value that maximizes the ductile behavior. This is perhaps counterintuitive, since one would assume that deformation occurring at higher temperatures, with lower strain rates, should produce the larger elongations to fracture. Also, fracture is anomalous because it is ordinarily neckless and occurs by the nucleation and interlinkage of bulk cavities.

Many polycrystalline solids whose grain size is stable and smaller than about 10 μm grain size exhibit superplastic behavior when the temperature and strain rate are kept within proper ranges. In the superplastic regime of deformation, the material can undergo large uniform strains prior to fracture.[2,3] Elongations of 10–20 times are quite common in superplastic samples subjected to uniaxial tensile stresses, and neck-free strains as large as 70–80 times have been reported.[4] The absence of internal residual stresses after distortion is another interesting property of the superplastic deformation because it is reminiscent of Pascal's law for fluid flow.

Although this phenomenon has been extensively investigated, there is in fact no existing theory which begins from the atomic, or grain, scale that permits a quantitative understanding in a unified way of the several features of superplastic flow. In particular, there is no clear-cut answer as to why the grains of a polycrystal become so prone to slide when the composition, temperature, and strain rates reach such precise conditions. Thus, superplasticity constitutes a challenge to solid-state theorists and, in spite of the large amount of empirical studies reported in the literature, the precise physical origin of superplastiity is still a mystery.

What we do know from experiments reveals that the temperature dependence of the superplastic strain rate for fixed stress follows a thermally activated law, with activation energy close to that of lattice diffusion.[5] Thus, vacancies have an important role in superplastic flow. However, a simple estimate demonstrates that the observed matter flow rates cannot be explained by merely a stream of vacancies in the opposite sense along the whole sample. Unreasonable concentrations would then be required. Therefore, although the motion of vacancies plays a principal role in the deformation, it is subsidiary to grain boundary sliding processes.

Most theoretical approaches reported in the literature extend the mechanisms of creep and assume that superplasticity is set in motion by grain boundary sliding accommodated by diffusional flow. The strain rate $\dot{\epsilon}$ turns out to be related to the applied stress σ by a power law $\dot{\epsilon}=A\sigma^n$.[6–17] However, this approach falls short because such a law does not fit the experimental data for constant n and does not shed light on other features of superplasticity. In particular, the most basic question as to why some alloys are superplastic, and others are not, has no clear-cut answer in current theories. The sin-

gular plastic characteristics, common to all superplastic materials, suggest that the phenomenon springs from a very basic origin, which still remains unclear.

Two recent advances seem to shine new light on the underlying atomic origin of superplasticity. Direct experimental evidence was supplied by Vetrano *et al.*[18,19] for the deformation-induced supersaturation of vacancies in the vicinity of many grain boundaries of a Al-Mg-Mn alloy during superplastic deformation. Rapid quenching of the sample while being superplastically deformed, by spraying a freon-type liquid on its surface, revealed the formation of nanocavities in 25% of the grain boundaries. The cavities produced in this manner are very unstable, quickly coalescing and disappearing after moderate heating. They are shown not to exist during deformation, but rather start forming after cooling and subsequent load release to polish and mount the sample in the transmission electron microscope.

They conclude that the presence of cavities provides evidence of a supersaturation of crystal vacancies near the sliding grain boundaries. The defects condense into voids when sliding abruptly ceases. Hence, vacancy excess is associated with the grain boundary sliding process. The supersaturation of vacancies is observed mainly in boundaries at 45° with respect to the tensile axis, where the shear stress is maximal, with near small particles intersecting the grain boundaries.

Vetrano *et al.* claim that boundary accommodation of two sliding crystallites involves the motion of dislocations with edges at the common boundary plane.[18] As real boundaries have in general complex shapes, the motion of the dislocations should combine glide and climb processes in order to respond to the accommodation demands. Climbing processes necessarily involve the release and capture of a large number of vacancies. Thus, the ability of the grain boundary to exchange these point defects has a rate-limiting role in the accommodation of sliding boundaries, even if one accepts that dislocations have the whole responsibility for the phenomenon. This explanation of the observed supersaturation of vacancies in superplastic deformation rests entirely on shape accommodation, and not on the sliding mechanism.

By the time of the publication of the papers of Vetrano *et al.*,[18,19] a novel mechanism for superplastic grain boundary sliding was put forward by the author[20] of this article, which clearly explains the general features and the role of vacancies in sliding. First, it begins by recognizing that the mechanical analysis of a stressed polycrystalline material must distinguish between intergranular and crystalline matter, because they have different mechanical properties and superplasticity does occur at the grain scale.[20,21] It is shown that a shear stress greater than a critical value applied in the plane of a nonideal grain boundary (having a step, intersecting hard particle, or triple junction) should buckle it, producing a periodic transversal deformation in the boundary.[20] This boundary corrugation induces a periodic normal stress field that alternates compression and traction on the surfaces of the adjacent crystal surfaces.

On the other hand, it is well known that grain boundaries are efficient sinks and sources for vacancies.[16] The concentration of crystal vacancies in equilibrium with the grain boundaries depends on the temperature and normal stress. Therefore, the periodic stress induced by the buckled boundary yields a periodic variation of the equilibrium value for the concentration of crystal vacancies. The grain boundary then evaporates and condenses the point defects in alternate sectors, producing streams of defects in closed loops that cross the boundary and involve the two adjacent crystals. These closed loops perform as the driving pulleys of a conveyor belt and the phenomenon provides both an accommodation mechanism and the driving force for crystal sliding.[20] Besides the remarkable quantitative agreement of the results with the temperature-dependent stress-strain rate experimental data for a number of alloys, the theory can also explain other phenomenological features of superplastic deformation. For example, it provides an insight for the causes of void nucleation and growth, observed in the superplastic deformation of many materials, and their prompt failure at high strain rates.

Most materials develop cavities during superplastic deformation. This fits the theory because it predicts that the sliding grain boundaries evaporate and condense vacancies in alternate, very close sectors. Normally, supersaturation of the point defects should not produce voids because they are rapidly captured after production. However, boundaries slide randomly during deformation. If a boundary suddenly stops sliding, both vacancy release and capture will cease as well, and the region near the boundary will remain supersaturated with vacancies. Then voids will start to nucleate.[22]

The explanation for the prompt fracture at high deformation rates is particularly interesting in the described scheme. The loop motion of vacancies, ascribed by the theory as the cause of superplasticity, explains remarkably well the experimental stress-strain rate curves even for very large strain rates, for which samples promptly fail. It seems contradictory that the alleged mechanism of superplastic deformation remains operative for strain rates where the effect is lost. However, the reduction of the final fracture elongation when the strain rate increases beyond the optimal value can be explained by the same mechanism. The overly rapid evaporation of vacancies at the grain boundaries produces high local concentrations of these defects and the consequent nucleation of them into rapidly growing coalescent voids, which weakens the sample. Additionally, it is shown here that superplastic properties must degrade either beyond the upper bounds of temperature and strain rate or for grain sizes too small.

This paper presents a more detailed account of the theory of Ref. 20, outlined above, and discusses several possibilities and properties that were not considered before. A new possible elastic instability of grain boundaries is studied, in addition to the corrugation effect discussed previously.[20] A closed-form constitutive equation relating stress, strain rate, temperature, grain size, and grain boundary thickness, with no undetermined or adjustable parameters, is derived from the theory. The agreement of this equation with experiment, over the whole range of these magnitudes essayed in the experiments, is excellent. The theoretical approach gives insight into the origin of some other phenomena, concurrent with superplastic distortion, such as cavitation, prompt failure at high strain rates, threshold stress, dependence on the grain size, and loss of superplasticity at high temperatures.

II. INTERACTION OF VACANCIES WITH GRAIN BOUNDARIES

One of the main hypotheses is that grain boundaries can be considered as perfect sources and sinks of crystal vacancies.[16] The structure of the atomic ordering close to a grain boundary is quite complex. Intergranular regions, or grain boundaries, are relatively wide layers, with typical thickness of several atomic distances. They couple two crystal structures oriented in different directions, with minimal deviation from crystal order. Such intermediate structure is required because any departure from the crystal ordering that minimizes the energy involves a very high local energy. The sudden change from one structure to the rotated one would involve a boundary surface with no crystal order and, hence, an energy per site far beyond the melting heat.

Dislocations have a principal role in the atomic structure of grain boundaries. Burgers[23,24] realized that, in order to attain minimal deviation from crystalline order, the space between two deviated crystallites should be filled by dislocations placed regularly, as wedges inserted between the crystal planes that gradually modify their orientation. Using this hypothesis, Read and Shockley[25] calculated the energy as a function of the angle between the crystals and obtained excellent agreement with experiment for small-angle grain boundaries. Grain boundaries of higher angles may be more complex, but in any event it is expected that dislocations will also play a principal role in their atomic structures. It is customary to consider intergranular matter as dislocation tangles that fill the space between the atomic planes at irregular angles.

However, a dislocation is a plane condensate of vacancies. Therefore, one can think of the grain boundary as a structure combining atoms and vacancies in a relatively ordered way. The fact that the vacancies constituting the grain boundary may be largely configured as dislocations is not important since an edge dislocation captures or releases lattice vacancies quite efficiently when climbing.[26] Hence, vacancies can be taken as its elementary constituents.

The picture of a grain boundary as a complex structure made of point defects raises the problem of the equilibrium of such a structure and its dependence on composition, temperature, and stress. Going a little further, one may think of intergranular matter in a polycrystalline solid as a thermodynamic phase of condensed vacancies.[27–29] In this manner, vacancies in the polycrystal can be either in free states, diffusing inside the crystallites, or condensed in the grain boundaries at a relatively uniform mean concentration. If the system is in thermodynamical equilibrium, then the two phases coexist and exchange vacancies reversibly and in equivalent rates; that is, the same number of defects are trapped by the boundary region and released by it, per unit time and unit area.

Changes in the local values of the thermodynamical variables—i.e., stress components, concentration of free vacancies, energy, or temperature—should result in a breaking of equilibrium, accompanied by the evaporation or condensation of vacancies at the interphases. The thermodynamics of such a system can be described as a lattice gas with a condensed phase. Its statistical mechanics has been fully worked out in the past, yielding an equilibrium equation.[27–29] However, there is a simpler way to derive this equation. Assume that the atomic concentration of vacancies diffusing in the crystals is η and the concentration in the condensed phase representing the grain boundary is denoted by the constant $1/\gamma$. Hence the grain boundary contains on average γ crystal sites, or $\gamma-1$ atoms, per vacancy. The condition for the thermodynamical equilibrium between the two phases, which is the physical situation describing a polycrystal, turns out to be[27–29]

$$\eta(1-\eta)^{\gamma-1} = \frac{1}{\kappa}\exp(-\beta\epsilon_B), \tag{1}$$

where ϵ_B is the binding energy of a vacancy in the grain boundary relative to the energy of a free defect, $\beta=1/(k_BT)$, k_B is the Boltzmann constant, and T is the absolute temperature. The numerical constant κ satisfies

$$1 < \kappa < 2 \tag{2}$$

and takes the values 1 and 2 in the two extreme cases of no shape entropy and unrestricted shape freedom, respectively.

Equation (1) has a very simple physical interpretation: at equilibrium, the two phases exchange defects reversibly. The rates of evaporation and condensation per unit area at the interphase must be the same. The rate of evaporation processes is proportional to the probability $(1-\eta)\exp(-\beta\epsilon_B)$ that a condensed vacancy is in front of a nonvacant crystal site, whose probability is $1-\eta$ and has the energy ϵ_B, necessary to go through the free phase. On the other hand, the rate of condensation events is proportional to the probability $\eta(1-\eta)^{\gamma}$ associated with the encounter of a free vacancy with γ nonvacant sites in a vicinity of the condensed phase. Except for the $1/\kappa$ factor, expression (1) results from equating these two probabilities. The coefficient $1/\kappa$ accounts for the possibility of events that create new condensed regions. If one assumes that the shape of the boundaries is stable and no additional condensed structures are created, then $\kappa=1$.

The equilibrium concentration η depends on the components σ_{ij}, where $i,j=x,y,z$, of the stress tensor through the dependence of ϵ_B on them. Generally, when considering a free and condensed vacancy in a stressed material, one may expect that the energy departure from their values in the unstressed condition is determined largely by the variation of the volume available. Consequently, $\epsilon_B=\epsilon(\Omega)$, where Ω is the volume per atom of the stressed crystallites. Thus, up to first order,

$$\epsilon_B(\Omega_0+\Omega_0\varepsilon_{ii}) = \epsilon_B(\Omega_0) - |\epsilon_B'|\Omega_0\varepsilon_{ii}, \tag{3}$$

where the summation convention over repeated indices is assumed, ε_{ij} denotes the strain tensor, ε_{ii} is the elastic dilation, and $\epsilon_B'=d\epsilon_B/d\Omega$, and Ω_0 represents the atomic volume of the undistorted crystal. The absolute value $|\epsilon_B'|$ was introduced because the volume derivative ϵ_B' is negative. Replacing Hooke's law

$$\sigma = B\varepsilon_{ii}, \tag{4}$$

where B is the bulk modulus, σ_{ij} represents the stress tensor, and σ is the hydrostatic tension,

$$\sigma = \frac{1}{3}\sigma_{ii}, \tag{5}$$

the equilibrium Eq. (1) becomes

$$\sigma = \frac{\epsilon_B}{\Omega^*} + \frac{k_B T}{\Omega^*}\ln[\kappa\eta(1-\eta)^{\gamma-1}], \tag{6}$$

where

$$\Omega^* = |\epsilon_B'|\frac{\Omega_0}{B}. \tag{7}$$

It is implicit in Eq. (4) that σ is positive for traction.

Equation (6) determines the relation between the thermodynamic variables at equilibrium and has a preeminent role in what follows. The grain boundaries capture or release vacancies when the temperature, concentration of vacancies, or stress departs from the equilibrium values given by Eq. (6) or when energy is provided. Isotropy is implicit in Eq. (4).

The equilibrium, Eq. (6), has an important consequence: as the grain boundaries perform as sources or sinks for vacancies, the diffusion equation does not hold there, and smooth stream lines of vacancies do occur only inside the crystallites. The exchange of vacancies among adjacent crystals occurs by stream lines which in general may change direction abruptly at the boundary. The component of the vacancy flux density vector $\vec{J}$ normal to the boundary, J_n, must be the same in the two sides; otherwise, the boundary region would increase or decrease indefinitely. The components parallel to the boundary may differ. Therefore, if the flux of vacancies changes direction at the grain boundary, the component of the density of flux parallel to the boundary has different values in the two sides of it and the two adjacent crystals will slide.

There is a more direct way expression (6) has a role in the deformation of a polycrystal.[20] For given temperature and local stress, Eq. (6) determines the concentration $\eta(\sigma,T)$ of vacancies the crystallites should have to be in equilibrium with the adjacent grain boundary. If the local normal stresses are not uniform and vary along the boundary, then σ and the equilibrium concentration should vary as well. The intergranular region will release or capture vacancies in order to reproduce the corresponding nonuniform equilibrium concentration $\eta(\sigma,T)$ in the vicinity of the boundary. The consequent concentration gradients will produce diffusive flow of vacancies, and matter, along the grain boundary.

III. MECHANICS IN THE GRAIN SCALE

In the macroscopic scale, for which the characteristic distances are always much larger than the grain size, the material is homogeneous and isotropic. Macroscopic stresses and strain fields change smoothly and undergo no significant variation in points separated by distances of the order of the grain size. However, at the grain scale the material is highly inhomogeneous because the mechanical properties of the grain boundaries and crystallites in general do differ. This inhomogeneity may induce intense stress fields that vary significantly from grain to grain, or inside grains, and average

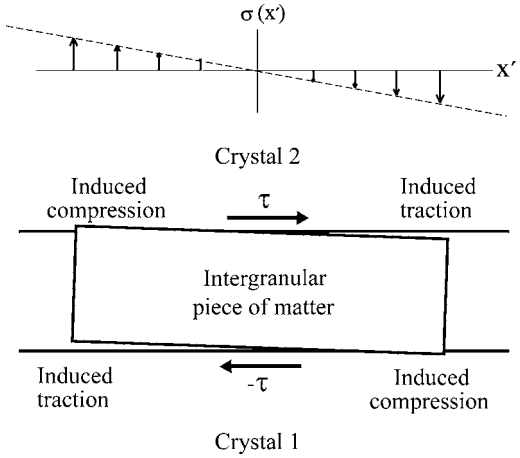

FIG. 1. Shear stress τ exerted in a section of the grain boundary delimited by two fissures. If intergranular matter performs as an elastic body, then a normal stress field $\sigma(x')$ is induced at the crystal surfaces.

to zero in a larger scale.[20,21] The granular metallographic structure may induce strongly varying stresses in the grain scale in a number of ways. The next subsections offer some examples.

A. Pinch and twist of grain boundary matter

Figure 1 illustrates an elementary mechanism by which the inhomogeneous nature of the stressed material may give rise to rapidly varying stress fields. The small piece of matter placed between the two grain surfaces 1 and 2 may represent a small crystallite or a sector of the intergranular matter. The main stress field caused by the forces external to the sample determines that the side crystals 1 and 2 exert a shear stress τ to the central piece. The shear forces are parallel to the plane of the boundaries. The system is in quasiequilibrium, and the torque exerted on the intergranular region by the shear forces parallel to the boundaries is equilibrated by the normal stress fields $\sigma_1(x')$ and $\sigma_2(x')$ induced in the two crystals 1 and 2. The x' axis is parallel to the boundary. Considering both crystals and the region in between as three elastic bodies, one concludes that the induced normal fields vary linearly with x'. The slope k of this linear relation can be determined replacing $\sigma = kx'$ in the equilibrium equation for the force momenta,

$$\int_{-d'/2}^{d'/2} x'\sigma\, dx' = \tau d' d_1, \tag{8}$$

where d' and d_1 are the dimensions of the central piece of matter in the directions parallel and perpendicular to the boundary, respectively. If it were a crystallite, d' and d_1 would be the grain size d. If the central body represents a piece of intergranular matter, d_1 is the grain boundary thickness. This way, solving Eq. (8) to obtain k,

$$\sigma_1 = \frac{12 d_1}{d'^2}\tau x', \quad \sigma_2 = -\frac{12 d_1}{d'^2}\tau x', \quad -d'/2 \leqslant x' \leqslant d'/2. \tag{9}$$

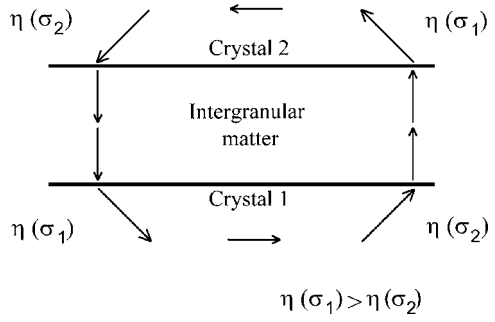

FIG. 2. The normal stress field induced in the two crystal surfaces modifies the equilibrium concentration $\eta(\sigma)$ of vacancies, determined by Eq. (6). Evaporation and condensation of vacancies from, and to, the grain boundary does occur, together with diffusive flow through the crystals. Lattice diffusion takes place in closed loops.

There is an important remark to add concerning the previous derivations. In a homogeneous material, the torque exerted by the shear forces parallel to the boundary, and associated with the stress component $\tau=\sigma_{x'z'}$ shown in Fig. 1, is equilibrated by the torque of the stress component $\sigma_{z'x'}$. The latter involves shear forces in the plane perpendicular to the boundary, along the z' axis. The induced normal stresses σ_1 and σ_2 appear in the supposed absence of these very forces. The elastic interaction of the central body with the rest of the material in the x' direction was simply neglected, as it were bounded by fissures in that direction. A justification for this procedure is given in the next section.

Both induced normal stress fields change sign at $x'=0$, as depicted in Fig. 1, which determines tractioned and compressed regions in crystals 1 and 2. Vacancies evaporate from the grain boundary in the tractioned areas, where Eq. (6) determines a higher equilibrium concentration η, and condense in the compressed regions, where the equilibrium concentration is lower. The stress variation along the x' direction induces a gradient in the concentration of vacancies and, consequently, diffusive flow parallel to the boundary in both crystals. The flow has opposite senses in the two crystals and the stream lines are essentially closed loops crossing the grain boundary, as shown schematically in Fig. 2. Lattice diffusion in closed loops between contiguous crystallites involves a relative motion, or sliding, of the two crystals. For future reference, the slope of the induced stress field along the grain surface is

$$\frac{d\sigma}{dx'}=\frac{12d_1}{d'^2}\tau. \tag{10}$$

B. Trench formation instabilities of grain boundaries

Interfaces in stressed solids were the subject of a recent study which shows that, in general, ideally planar structures in bulk polycrystalline materials become rough when subjected to strong enough in-plane shear forces.[30] This effect is clearly a bulk analog of the Asaro-Tiller-Grinfeld instability—i.e., the stress-induced buckling of solid surfaces into trenches or islands[31–33]—and also of the spontaneous roughening of thin films produced by large in-plane stresses arising from lattice mismatch with the substrate.[34–39] This mismatch originates an in-plane shear on the film, and the consequent bending torque accumulates to a length at which the film buckles and corrugates or collapses into trenches. These two related surface effects are of practical importance and have received considerable attention.

The Asaro-Tiller-Grinfeld instability of surface layers, or films on substrates, is well established by theory, computer simulation, and experiment. The mechanical analysis of a planar structure inside a stressed solid, like a grain boundary, does not differ essentially from that of a surface layer, and hence a similar elastic instability should be expected in it. In effect, using a Monte Carlo simulation and analytical treatment, Bellon and Averback[30] show that bulk interfaces and grain boundaries under overcritical in-plane stress undergo an elastic instability, followed by atomic transport driven by the induced stress fields. The bulk effect is more complex than its surface counterpart, since the elastic instability is followed by a structural one. The experimental observations of the surface instabilities[36,39,40] provide indirect experimental support to the bulk effect, which has the same physical origin but is more difficult to detect experimentally.

The continuous mechanical model introduced in Ref. 20 will be reviewed and employed in the next sections to show that the boundary separating two crystallites may become elastically unstable when subjected to an overcritical shear stress. The instability may produce two effects: a periodic trenching should always occur in a sheared infinite plane layer immersed in an elastic medium, but a concurrent in-plane compression may induce a corrugation which inhibits trenching. For the purposes of the present analysis, the main consequence of both effects is the rise of periodic normal stress fields in the two adjacent crystal surfaces. According to Eq. (1), these periodic stress fields should modify the local thermodynamic equilibrium of vacancies in the interfaces between the two crystals and the intergranular matter.

The hypothesis is that in a polycrystal subjected to external forces, the mechanical analysis must distinguish intergranular and crystalline matter as separate units because they have slightly different mechanical properties.[20,21] Intergrain matter is assimilated into a thin elastic plate immersed in a different elastic medium representing the crystals. The two contiguous crystallites exert shear forces on the plate representing the intergrain matter. These shear forces are in the plane of the elastic plate of thickness d_1, width b, and length L and are parallel to the main direction, which is the dimension of length L. The corresponding shear stress is denoted τ.

Up to this point the model is incomplete because lacks an in-plane compressing force, which is expected to occur in any real grain boundary under shearing. In effect, a pure shear exerted by the two crystallites on the intergrain region may be partially transformed into in-plane compression by geometric imperfections in the crystallite surfaces, like interface steps, second phase inclusions, or particles and triple junctions. To take this into consideration, two compressing in-plane forces of strength F, parallel to the main dimension as well, are applied to the edges of size b of the plate. Only the main dimension and transversal deformations, normal to the plane of the plate, will be considered. The magnitudes b and L will not appear in the final solution.

The elastic plate modeling the grain boundary is immersed in a solid medium with different elastic constants, representing crystalline matter. In this way, if a section δx of the plate, at distance x from the left end along the main dimension, undergoes a transversal shift $y(x)$, then the elastic medium will exert on it a restitutive force $-2\alpha y(x)b\ \delta x$, where 2α is a constant proportional to the Young's modulus of the crystals. If $F=\tau=0$, the undeformed plate remains plane.

The shape function $y(x)$ of the plate is governed by the following general equation, originally attributed to Euler and commonly used in materials mechanics to calculate shapes of loaded beams:

$$\frac{y''}{(1+y'^2)^{3/2}} = -\frac{M(x)}{EI}, \tag{11}$$

where E denotes Young's elasticity modulus of the plate and I the moment of inertia of the transversal section. The function $M(x)$ stands for the moment of the forces applied in the interval $[0,x]$ with respect to the point x of the plate. The left-hand side of Eq. (1) is the curvature at x—i.e., the inverse of the radius of the osculating circle. By replacing, in Eq. (11), $M(x)$ with the total moment of the forces τbx, F and $-2\alpha by(x)$, one obtains for $y(x)$ the integro-differential equation[20]

$$\frac{y''}{(1+y'^2)^{3/2}} = \frac{\tau b d_1}{EI}x - \frac{F}{EI}(y-y_0) - \frac{2\alpha b}{EI}\int_0^x y(x')(x-x')dx' - \frac{M_0}{EI}, \tag{12}$$

where $y_0=y(0)$ and M_0 is an external moment applied at $x=0$.

By simply examining Eq. (12) with the physical meaning of its terms in mind, one can conclude that a long plate cannot be stable and would collapse into strips if τ is big enough. In effect, the second and third terms of the right-hand side of Eq. (12) are bounded because any physical solution for the transversal displacement $y(x)$ has finite limits. However, the first term increases indefinitely with x and, consequently, the whole right-hand side of the equation is not bounded if x is not bounded as well. Therefore, the curvature of $y(x)$, represented by the left-hand side of Eq. (12), can reach values as high as desired for a large enough $|x|$.

To put this in a more quantitative fashion, assume that the shear stress τ is large and the elastic medium in which the plate is immersed is very stiff. In such a situation, it is expected that the transversal deformation $y(x)$ is small for any x in $[0,L]$ and the first term on the right-hand side of Eq. (12) is dominant. The resulting approximate equation

$$\frac{y''}{(1+y'^2)^{3/2}} = \frac{\tau b d_1}{EI}x - \frac{M_0}{EI} \tag{13}$$

can be solved exactly. The first integration gives

$$y'(x) = \frac{\frac{\tau b d_1}{EI}x^2 - C}{\sqrt{1-\left(\frac{\tau b d_1}{EI}x^2 - C\right)^2}}, \tag{14}$$

with

$$C = -\frac{y_0'}{\sqrt{1+y_0'^2}} \tag{15}$$

and $y_0'=y'(0)$ is the slope at the origin. It is evident from Eq. (15) that $|C|<1$. The slope $y'(x)$ of the displacement function is real for

$$|x| \leqslant \ell = \sqrt{\frac{2EI}{\tau b d_1}\left(1+\frac{|y_0'|}{\sqrt{1+y_0'^2}}\right)} \tag{16}$$

and $|y'(\pm\ell)|=\infty$. The maximum transversal displacement occurs at

$$x_0 = \pm\sqrt{\ell^2 - \frac{2EI}{\tau b d_1}}, \tag{17}$$

where $y'(x_0)=0$. Therefore, the plate modeling the grain boundary is expected to break at points x_1, with $|x_0|<|x_1|<\ell$, and develop a periodic structure of parallel fissures, or trenches, whose period is approximately 2ℓ. Replacing $y_0' \approx 0$ and the moment of inertia

$$I = \frac{d_1^3 b}{12} \tag{18}$$

in Eq. (16), one obtains for the ratio of the semiperiod ℓ between trenches and the grain boundary thickness d_1:

$$\frac{\ell}{d_1} \approx \sqrt{\frac{E}{6\tau}}. \tag{19}$$

Placing $E\approx 10^5$ MPa and $\tau\approx 1$ MPa one obtains $2\ell=260d_1$.

At this point, it may be helpful to offer a more pictorial example of the situation described above. Consider two bodies with two plane faces stuck by a thin film of glue of thickness d_1. Shear forces parallel to the plane faces applied to the bodies make the glue collapse when they are high enough to make 2ℓ smaller than the dimension d of the body faces. In that moment, the glue develops trenches whose edges start to curl. Therefore the in-plane shear stress τ has a threshold

$$\tau_c = \frac{2E}{3}\left(\frac{d_1}{d}\right)^2, \tag{20}$$

which follows from replacing $2\ell=d$ in Eq. (19).

The sectors between trenches of a collapsed grain boundary can be identified with the central piece of matter referred to in the previous section and appearing in Fig. 1. The present analysis explains why the shear stress $\sigma_{z'x'}$ was omitted in the equilibrium equations in that section. Once the transversal fissures are produced in the boundary, the local

shear stresses $\sigma_{z'x'}$ disappear and the induced normal stresses $\sigma_1(x')$ and $\sigma_2(x')$ arise to equilibrate the in-plane shear forces associated with $\sigma_{x'z'}$.

C. Buckling and corrugation of grain boundaries

In addition to the trenching effect of the previous section, there is another class of mechanical instability of grain boundaries which was already considered in connection with superplasticity.[20] Assume a class of solutions of Eq. (12) for which $y'(x) \ll 1$ for any x in $[0,L]$. Then the equation can be simplified to

$$y'' = \frac{\pi b d_1}{EI} x - \frac{F}{EI}(y - y_0) - \frac{2\alpha b}{EI}\int_0^x y(x')(x - x')dx' - \frac{M_0}{EI}, \tag{21}$$

which admits the solution

$$y(x) = \delta \sin(kx), \tag{22}$$

provided that $M_0 = y_0 = 0$,

$$k^4 - \frac{F}{EI}k^2 + \frac{2\alpha b}{EI} = 0, \tag{23}$$

and

$$\pi d_1 = \frac{2\alpha\delta}{k}. \tag{24}$$

Equations (23) and (24) determine the periodicity $2\ell' = 2\pi/k$ and amplitude δ of the solution. However, Eq. (23) has real solutions for k only when $F \geqslant 2\sqrt{2\alpha b EI} \equiv F_c$. Therefore, the existence of sinusoidal solutions demands an in-plane compressing force F greater than the critical value F_c.

The coefficient k also has a minimal value, given by

$$k_{\min}^2 = \sqrt{\frac{2\alpha b}{EI}}, \tag{25}$$

which determines a stress independent maximum for the semiperiod ℓ'.

It is illustrative to make an estimation of ℓ' to compare with the semiperiod ℓ of the trenching effect considered before. By substituting in Eq. (25) $\alpha = E'/d$ and the explicit expression for the moment of inertia (18), where E' is the Young's modulus of the crystallites and d the grain size, one obtains that the semiperiod $\ell' = \pi/k$ of the sinusoidal solution has an upper bound:

$$\ell' \leqslant \pi\left(\frac{d\, d_1^3 E}{24E'}\right)^{1/4}. \tag{26}$$

Taking $E' \approx E, d = 10^{-3}$ [cm] and estimating the grain boundary thickness as $d_1 \approx 3 \times 10^{-7}$ [cm], Eq. (26) gives $\ell'(\max) \approx 10^{-6}$ [cm] $= 10^{-2}$ [μm] for the semiperiod of the corrugational buckling effect.

For the same value of d_1 the semiperiod of the trenching instability turns out to be $\ell \approx 4 \times 10^{-5}$ [cm] $= 0.4$ [μm]—that is, about 40 times greater than the semiperiod of ondulational buckling.

Hence, a sheared grain boundary subjected to a concurrent in-plane compressing force F greater than the critical value F_c should periodically distort the boundary with semiperiod ℓ'. The relevant conclusion is that the boundary distortion induces a periodic normal stress field

$$\sigma_1(x) = \pm \alpha\delta \sin\left(\frac{\pi}{\ell'}x\right) \tag{27}$$

in the surfaces of the two adjacent crystallites. The positive sign applies to one of the crystal surfaces and the minus sign applies to the other. In effect, for each value of x the stresses in the two crystal surfaces have opposite signs. If one of the crystals is compressed by the transversal displacement of the grain boundary, the other one is tractioned.

IV. MATTER FLOW INDUCED BY THE GRAIN BOUNDARY MECHANICAL INSTABILITIES AND STRAIN RATE TENSOR

When identifying the central piece of matter in Figs. 1 and 2, referred to in Sec. III A, with a sector of the grain boundary between two trenches, then $d' = 2\ell$ and the stress fields (9) induced in the two adjacent crystals read

$$\sigma_1 = \frac{3d_1}{\ell^2}\pi x', \quad \sigma_2 = -\sigma_1, \quad -\ell \leqslant x' \leqslant \ell. \tag{28}$$

The concentration of vacancies in the two crystal surfaces, in equilibrium with the common grain boundary, are $\eta[\sigma + \sigma_1(x')]$ and $\eta[\sigma - \sigma_1(x')]$. Hence the variation of the normal stresses in the two crystal surfaces determines concentration gradients in them. These gradients drive opposed currents of vacancies near the crystal surfaces, as shown schematically in Fig. 2. The flow of crystal vacancies implies matter flow in the opposite sense and the two crystals will slide. Now there is the issue of evaluating the relative speed of the two adjacent crystallites.

Taking gradient of Eq. (1) and making use of the same equation to reduce the resulting expression, one obtains

$$\frac{1 - \gamma\eta}{\eta(1 - \eta)}\nabla\eta = -\beta\nabla\,\epsilon_B. \tag{29}$$

The density η/Ω_0 of crystal vacancies close to the grain boundary, where Ω_0 is the volume per atom, is related with the vector density of flux $\vec{J}_v$ of the vacancy stream by

$$\vec{J}_v = -\frac{D}{\Omega_0}\nabla\eta, \tag{30}$$

where D is the diffusion coefficient for vacancies. Substituting this and

$$\nabla\epsilon_B = -\Omega^*\nabla\sigma, \tag{31}$$

Eq. (29) turns into

$$\vec{J}_v = -\frac{D}{k_B T}\frac{\Omega^*}{\Omega_0}\frac{\eta(1 - \eta)}{1 - \gamma\eta}\nabla\sigma. \tag{32}$$

This expression determines the flow of vacancies parallel, and close, to a crystal boundary, produced by a normal stress

gradient. However, physically, the stream of vacancies can be thought of as an opposite flux of atoms, whose vector flow density

$$\vec{J}_{\text{lattice}} = \frac{1}{\Omega_0}\vec{v}, \tag{33}$$

where $1/\Omega_0$ represents the atomic density and $\vec{v}$ the mean atomic drift velocity, satisfies $\vec{J}_{\text{lattice}} = -\vec{J}_v$. Combining this with Eqs. (32) and (33) one obtains

$$\vec{v} = -\frac{D}{k_B T}\frac{\eta(1-\eta)}{1-\gamma\eta}\Omega^* \nabla \sigma. \tag{34}$$

Applying Eq. (34) to the two adjacent crystal surfaces and recalling that because of Eqs. (28) the derivative of the normal stresses in the surfaces of the contiguous crystals are

$$\frac{d\sigma_1}{dx'} = \pm \frac{3d_1}{\ell^2}\tau, \tag{35}$$

it follows that the relative speed between two adjacent crystallites is

$$\Delta v = \frac{6d_1}{\ell^2}\frac{D}{k_B T}\frac{\eta(1-\eta)}{1-\gamma\eta}\Omega^* \tau. \tag{36}$$

The next step is the transformation of Eq. (36) into a practical equation relating the flow stresses to the strain rate. To accomplish this task, it is necessary to better define the frames of references. Let (xyz) be the main frame of reference, whose axes are parallel to the principal directions of the stress tensor. The principal stresses are σ_x, σ_y, and σ_z. Figure 3 shows an elementary section of the material, much longer in the z direction, that cuts a large number n of grain boundaries in that direction (in Fig. 3, $n=4$ because of the space available). Each boundary differentiates two crystals that slide with relative velocity $\Delta\vec{v}$. The local frame of reference $(x'y'z')$ is rotated so that the $x'y'$ plane is in a grain boundary surface. According to Eq. (36), the components of $\Delta\vec{v}$ in the rotated frame of reference are

$$\Delta v_{i'} = \mathcal{Q}\,\sigma_{i'z'}, \quad \Delta v_{z'} = 0, \quad i' = x', y', \tag{37}$$

where the shear stress appearing in Eq. (36) was written in the more precise notation $\tau = \sigma_{i'z'}$ and

$$\mathcal{Q} \equiv \frac{6d_1}{\ell^2}\frac{D}{k_B T}\frac{\eta(1-\eta)}{1-\gamma\eta}\Omega^*. \tag{38}$$

The example of Fig. 4 shows the relation between the relative velocities between a number of contiguous crystals along the z direction and the components $\dot{\varepsilon}_{iz}$ of the strain rate in the main system of reference, where

$$\dot{\varepsilon}_{iz} = \frac{1}{nd}\sum_{p=1}^{n} \Delta v_i(p), \quad i = x, y, z, \tag{39}$$

where the sum runs over a series of n grain boundaries along the z axis, p enumerates the boundaries, and $\Delta v_i(p)$ denotes the i component of the relative velocities of the pair of crystallites with a common boundary p. Equation (39) can be written as

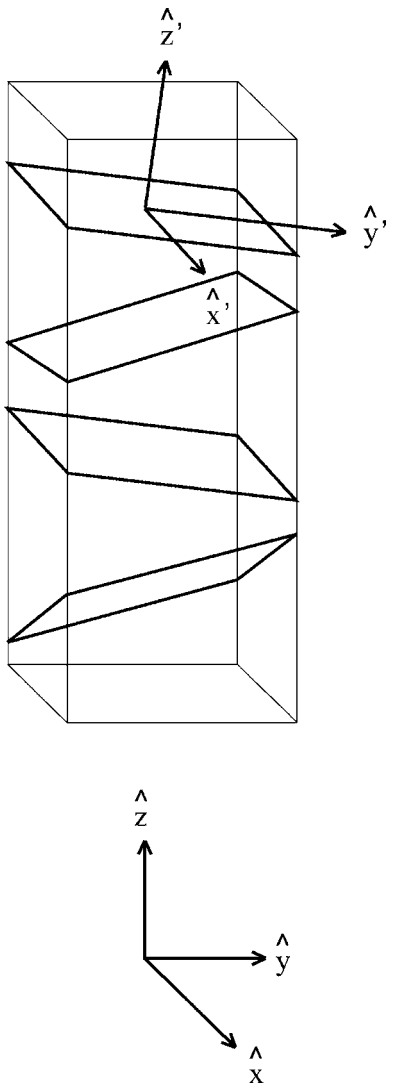

FIG. 3. A narrow section of the material, supposedly much longer in the z direction, cuts many boundary planes. The local frame of reference $(x'y'z')$ associated with one of these planes is shown.

$$\dot{\varepsilon}_{iz} = \frac{1}{d}\langle \Delta v_i \rangle_z, \quad i = x, y, z, \tag{40}$$

where $\langle \Delta v_i \rangle_z$ is the projection of the relative slide velocity on the i axis of the main frame of reference (xyz), averaged over all orientations of the boundary. Notice that the average must keep the normal to the boundary plane (the z' direction) in the semispace $z \geqslant 0$. Therefore, to obtain an expression for $\dot{\varepsilon}_{iz}$ we must express the relative velocities given by Eq. (37) in the principal frame of reference (xyz), and then average over all directions of the local frame $(x'y'z')$ with z' in the upper semispace.

Despite the fact that the components of the relative velocity $\Delta\vec{v}$ are defined in Eq. (37) in terms of the components of the stress tensor, it is actually a vector and transforms as one. As the axes of the main frame of reference are oriented in the principal directions of the stress tensor, in the main frame

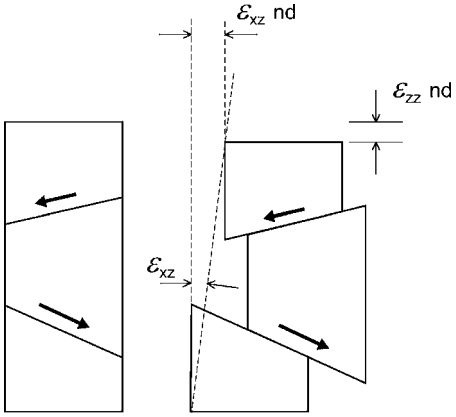

FIG. 4. The narrow section of the material, supposedly much longer along the z axis, that cuts $n=3$ crystals in that direction is shown in two instants. Sliding of the boundary surfaces causes plastic strains. The strain rates $\dot{\varepsilon}_{zz}$ and $\dot{\varepsilon}_{xz}$ are proportional to the sum of the relative velocities projected over the z and x axes. Equations (39) and (40) follow.

this tensor is diagonal and reads $(\sigma_i\delta_{ij})$. The principal stresses σ_i are assumed to be the input data. Hence, the first step for obtaining the components Δv_i in the main frame (xyz) is the transformation of $(\sigma_i\delta_{ij})$,

$$(\sigma_{i'j'}) = R(\theta,\phi)\begin{pmatrix}\sigma_x & 0 & 0\\ 0 & \sigma_y & 0\\ 0 & 0 & \sigma_z\end{pmatrix}R^T(\theta,\phi), \tag{41}$$

to express it in the rotated local frame $(x'y'z')$. In Eq. (41), $R(\theta,\phi)$ is the rotation matrix associated with the transformation $(xyz)\rightarrow(x'y'z')$. The angles θ and ϕ are the corresponding Euler angles. Explicitly, $R(\theta,\phi)$ reads

$$R(\theta,\phi) = \begin{pmatrix}\cos\phi & \sin\phi & 0\\ -\sin\phi\cos\theta & \cos\phi\cos\theta & \sin\theta\\ \sin\phi\sin\theta & -\cos\phi\sin\theta & \cos\theta\end{pmatrix}, \tag{42}$$

when the rotated x' axis remains in the xy plane, forming an angle ϕ with the x axis, and the other Euler angle θ is the angle between the rotated z' and old z axes. The angles θ and ϕ are such that the normal to the plane of the grain boundary is given by the unit vector

$$\hat{n}' = \begin{pmatrix}\sin\phi\sin\theta\\ -\cos\phi\sin\theta\\ \cos\theta\end{pmatrix}. \tag{43}$$

Once the tensor $(\sigma_{i'j'})$ is obtained, the relative velocities (37) in the rotated frame can be constructed explicitly from the components $\sigma_{i'z'}$ $(i'=x',y')$ of the rotated tensor. These are

$$\sigma_{x'z'} = (\sigma_x-\sigma_y)\sin\phi\cos\phi\sin\theta,$$

$$\sigma_{y'z'} = -(\sigma_x\sin^2\phi+\sigma_y\cos^2\phi-\sigma_z)\sin\theta\cos\theta. \tag{44}$$

The average of the relative velocities is calculated performing first the inverse transformation

$$\begin{pmatrix}v_x\\ v_y\\ v_z\end{pmatrix} = R^T(\theta,\phi)\begin{pmatrix}v_{x'}\\ v_{y'}\\ 0\end{pmatrix}, \tag{45}$$

to express $\Delta\vec{v}$ in the main coordinate axes, and then integrating the Euler angles θ and ϕ over the semispace $z>0$, in this way taking into account all possible orientations of the boundary planes. The procedure is rather tedious but straightforward. Skipping the details, the relative velocity between sliding crystallites turns out to be

$$\Delta\vec{v} = \mathcal{Q}\begin{pmatrix}(\sigma_x-\sigma_y)\sin\phi\cos^2\phi\sin\theta+(\sigma_x\sin^2\phi+\sigma_y\cos^2\phi-\sigma_z)\sin\phi\sin\theta\cos^2\theta\\ (\sigma_x-\sigma_y)\sin^2\phi\cos\phi\sin\theta-(\sigma_x\sin^2\phi+\sigma_y\cos^2\phi-\sigma_z)\cos\phi\sin\theta\cos^2\theta\\ -(\sigma_x\sin^2\phi+\sigma_y\cos^2\phi-\sigma_z)\sin^2\theta\cos\theta\end{pmatrix}. \tag{46}$$

The components of the average sliding velocity

$$\langle\Delta\vec{v}\rangle_z = \frac{1}{\pi^2}\int_0^{\pi/2}d\theta\int_0^{2\pi}d\phi\,\Delta\vec{v}(\theta,\phi), \tag{47}$$

expressed as the z components of the strain rate tensor, take the simple form

$$\dot{\varepsilon}_{xz}=0,\quad \dot{\varepsilon}_{yz}=0,\quad \dot{\varepsilon}_{zz}=\frac{\mathcal{Q}}{3\pi d}(-\sigma_x-\sigma_y+2\sigma_z). \tag{48}$$

The other components of the strain rate tensor are analogous. Writing the latter in full and replacing the explicit expression (38) for $\mathcal{Q}$ one finally has

$$(\dot{\varepsilon}_{ij}) = \frac{2d_1}{\pi d\ell^2}\frac{D(T)}{k_BT}\frac{\eta(\sigma)[1-\eta(\sigma)]}{1-\gamma\eta(\sigma)}\Omega^* \times\begin{pmatrix}2\sigma_x-\sigma_y-\sigma_z & 0 & 0\\ 0 & -\sigma_x+2\sigma_y-\sigma_z & 0\\ 0 & 0 & -\sigma_x-\sigma_y+2\sigma_z\end{pmatrix}. \tag{49}$$

The explicit dependence of the strain rates on the principal stresses σ_i is obtained combining Eqs. (6) and (49). Considering that the atomic concentration satisfies $\eta\ll 1$, Eq. (6) reduces to the much simpler expression

$$\eta = \frac{1}{\kappa}\exp\left(-\frac{\varepsilon_B - \Omega^*\sigma}{k_B T}\right). \tag{50}$$

Replacing as well a thermally activated expression for the diffusion coefficient,

$$D(T) = D_0 \exp\left(-\frac{\epsilon_a}{k_B T}\right), \tag{51}$$

one finally obtains

$$(\dot{\varepsilon}_{ij}) = \frac{2d_1}{\pi\kappa d\ell^2}\frac{D_0}{k_B T}\exp\left(-\frac{\epsilon_a + \epsilon_B}{k_B T}\right)\exp\left(\frac{\Omega^*}{k_B T}\sigma\right)\Omega^* \times \begin{pmatrix} 2\sigma_x - \sigma_y - \sigma_z & 0 & 0 \\ 0 & -\sigma_x + 2\sigma_y - \sigma_z & 0 \\ 0 & 0 & -\sigma_x - \sigma_y + 2\sigma_z \end{pmatrix}. \tag{52}$$

As expected, $\dot{\varepsilon}_{ii}=0$, which means that volume remains unchanged in the deformation. In Eqs. (50) and (52) $\sigma=(\sigma_x+\sigma_y+\sigma_z)/3$ is the hydrostatic tension.

There is an important aspect to clarify at this point. Notice that, although Eq. (19) indicates that ℓ does depend on the local shear stress τ, this magnitude was taken as a constant in the derivations that follow. If Eq. (19) for ℓ were replaced in Eq. (38) for $\mathcal{Q}$, then the relative velocity given by Eq. (37) would be quadratic in the stresses, instead of linear. The point is crucial since Eq. (37) constitutes the starting point in the derivation of the strain rates (52). The distance 2ℓ between trenches was assumed as a stress-independent constant because the stress-induced trenching is a phenomenon previous in time to the deformation and boundary sliding. In this theory, the latter is an effect of the former. On the other hand, a fissure in the grain boundary should remain at the point where it was formed and should not be able to promptly displace to respond to variations of the shear stress which produced it initially, particularly because the dependence of ℓ on the stress τ is rather weak, as shown by Eq. (19).

Therefore, by the physical arguments given above, we can assume that grain boundaries buckle into periodic trenches for in-plane shear stresses greater than the critical value given by Eq. (20). The period 2ℓ between trenches is commensurate with the grain boundary face and remains fixed, irrespective of the applied stress, provided that it is greater than the critical one. This assumption has proven to be sound because Eq. (52) gives an excellent agreement with the experimental results, as is shown in a forthcoming section. Instead, no reasonable fit of the data can be attained with a quadratic dependence on the tensile stress.

The analysis of this section gives all credit to the splitting of grain boundaries into sections by the apparition of trenches at a critical in-plane shear stress, explained in Sec. III B. It differs from that given in Ref. 20 in that the latter considers only the corrugation effect, reviewed in Sec. III C. Formally, the final result for the strain rate tensor obtained in that previous paper[20] differs from Eq. (52) only in a numeric factor of the order of unity. The coefficient $2/(\pi\kappa)$ of Eq. (52) should be replaced by $\pi/3$ to recover the corresponding expression of Ref. 20. (In the latter it was assumed $\kappa=2$.) However, the two theories have deep physical differences. The main difference is the meaning of the semiperiod ℓ appearing in the two results. As was discussed in Sec. III, the semiperiod ℓ of the trench formation effect is expected to be about 40 times larger than ℓ', the semiperiod of the corrugation effect of Sec. III C and Ref. 20.

V. THRESHOLD STRESS AND DEPENDENCE ON GRAIN SIZE

The trench formation effect involves a threshold for the in-plane shear stress

$$\tau = \sqrt{\sigma_{x'z'}^2 + \sigma_{y'z'}^2} \tag{53}$$

exerted on a grain boundary face. In effect, Eq. (19) shows that the distance 2ℓ between two trenches decreases for increasing τ. If $2\ell > d$, the grain size being d, no fissure can occur. When τ increases and reaches a critical value τ_c, given by Eq. (20) for which $2\ell=d$, trenches start to develop at the extremes of the grain boundary into consideration. The mechanism of boundary sliding then becomes operative.

For uniaxial tensile stress σ_z along the z axis, $\sigma_x=\sigma_y=0, \sigma=\sigma_z/3$ and Eq. (52) can be written as

$$\dot{\varepsilon} = C_0\frac{\Omega^*(\sigma_z - \sigma_0)}{k_B T}\exp\left(-\frac{\epsilon_0 - \frac{1}{3}\Omega^*\sigma_z}{k_B T}\right), \tag{54}$$

where $\dot{\varepsilon}=\dot{\varepsilon}_{zz}$,

$$\epsilon_0 \equiv \epsilon_a + \epsilon_B, \tag{55}$$

and the coefficient C_0 is given by

$$C_0 = \frac{4d_1 D_0}{\pi\kappa d\ell^2}. \tag{56}$$

The energy ϵ_0 is the activation energy for the exchange of vacancies between the crystal and grain boundary region. In effect, ϵ_a is the energy barrier for such point defect between two bulk crystal sites and ϵ_B is the energy difference between vacancies at equilibrium in the perfect crystal and grain boundary. Hence, the sum ϵ_0 is the height of the barrier a vacancy has to overcome to evaporate from the boundary to the crystal.

Equation (54) is not exactly a particularization of the result (52) because it incorporates a threshold stress σ_0 substracted to σ_z in the preexponential factor.[22] The derivation of Eq. (52) assumes from the beginning that the grain boundaries are buckled, which actually occurs only when the in-plane shear stresses (53) exerted on the boundaries exceed the critical value. Therefore, Eq. (52) overestimates the deformation rate $\dot{\varepsilon}$ for small stresses. A simple way to correct this is by introducing the threshold term σ_0. By virtue of it, Eq. (54) predicts that the strain rate vanishes for a finite applied stress $\sigma_z=\sigma_0$. At any rate Eq. (52) and its modified version (54) may overestimate a bit the strain rate. In effect, the shear stress vanishes in surfaces normal to the principal axes. Therefore, no matter how strong the externally applied force may be, there are always some grain boundaries for which the shear stress is below the critical value τ_c, simply

because their normals are close to a principal axis. However, the average (47) considers all orientations in the same footing.

The excellent agreement of Eqs. (54) and (56) with a great amount of highly reliable experimental data opens a rather puzzling issue. In effect, Eq. (54) reproduces within the experimental uncertainties the results of tensile tests conducted for a variety of aluminum, titanium, and copper superplastic alloys, over the whole range of strain rates and temperatures tested in the experiments. An example of this remarkable agreement between Eq. (54) and the published experimental data on superplastic deformation is provided in Ref. 20 and in a forthcoming section of this paper. In addition, adjusting the coefficient C_0 to make Eq. (54) fit the experimental curves, one obtains excellent consistency with Eq. (56) for a reasonable choice of d_1, D_0 from tables, experimental d, and $\ell = 130 d_1$, as was estimated from Eq. (19).

Although the comparison between theory and experiment is the matter of a subsequent section, advancing a comment here is in order to take note of a paradox contained in the results written above. While Eqs. (54) and (56) give a noticeably precise numerical concordance with the experimental facts for fixed d, Eq. (56) predicts a d^{-1} dependence on the grain size. This contradicts most authors, who claim that the superplastic strain rate varies as d^{-p}, with $2 \leqslant p \leqslant 3$. Moreover, it will be shown later that Eq. (54) fits the experimental data on the superplastic deformation of samples with different grain sizes for C_0 proportional to d^{-3}.

However, the failure of Eq. (56) in giving the right dependence of C_0 on the grain size d is not real. It can be explained by the already mentioned rigidity of ℓ to respond to the shear stress applied to the grain boundary and the condition that 2ℓ must be commensurate with d in each boundary face. When the critical shear stress (20) is just surpassed, a fissure arises close to each of the two triple junctions in the verges of the boundary plane. If the in-plane shear stress τ is increased continuously, the situation does not vary promptly. The trenches just formed do not move and no new fissure emerges because 2ℓ must be commensurate with d. The boundary face splits into two sections by a central trench only when the in-plane stress reaches the new critical value

$$\frac{8E}{3}\left(\frac{d_1}{d}\right)^2 = 4\tau_c, \tag{57}$$

which follows from replacing $2\ell = d/2$ in

$$\tau = \frac{E}{6}\left(\frac{d_1}{\ell}\right)^2. \tag{58}$$

Hence the situation remains stationary for $\tau_c < \tau < 4\tau_c$, and just when the in-plane stress τ exceeds $4\tau_c$, the boundary surface splits into two sections. In turn, each of these sections splits into two parts after the shear stress becomes higher than $16\tau_c$ and so on. In general,

$$\ell = \frac{d}{2^n} \quad \text{for } 4^{n-1}\tau_c < \tau < 4^n\tau_c, \quad n = 1,2,\ldots, \tag{59}$$

$2^{(n-1)}$ being the number of sectors separated by parallel trenches in which the grain boundary face splits.

To realize the importance of this effect, an example is in order. For aluminum ($E = 7 \times 10^{10}$ Pa) of $d = 10$ μm and estimating $d_1 = 3 \times 10^{-7}$ cm (ten atomic distances), Eq. (20) gives $\tau_c = 4.2 \times 10^3$ Pa. For $n = 5$ relation (57) indicates that

$$2\ell = \frac{d}{16} \quad \text{for } 1 \text{ MPa} < \tau < 4 \text{ MPa},$$

$$2\ell = \frac{d}{32} \quad \text{for } 4 \text{ MPa} < \tau < 16 \text{ MPa}. \tag{60}$$

The example shows that the stress applied to a sample may vary over a wide range without affecting the magnitude of ℓ in the different grain boundary faces. The same applies to the grain size d, which can vary in a relatively wide range without modifying n and ℓ.

Therefore, one can substitute $\ell = d/2^n$ and write

$$C_0 = \frac{16\langle \nu \rangle^2 d_1 D_0}{\pi \kappa d^3}, \tag{61}$$

where $\langle \nu \rangle = \langle 2^n \rangle$ is twice the number 2^{n-1} of trenches in a buckled grain boundary face averaged over a large number of these faces. Equation (61) expresses the physics of the system better than Eq. (56) because it incorporates the fact that 2ℓ is commensurate with d through a very stable integral number. The relation (59) turns into

$$\frac{1}{4}\langle \nu \rangle^2 \tau_c \leqslant \tau \leqslant \langle \nu \rangle^2 \tau_c, \tag{62}$$

which determines the interval in which the shear stresses τ can vary without changing the local value of ν.

Irrespective of the strength of the principal stresses σ_i, the shear stress τ exerted on the boundary faces of the different grains varies from zero, for boundary planes normal to the principal directions, up to the maximum. Hence n always runs from zero to the maximum value determined by relation (59), which causes the average $\langle \nu \rangle$ to be a smooth, slowly varying function of σ_i and d. Any modification of the number of grain boundary trenches demands an increase of the shear stress in about 4 times. Further refinement of Eqs. (54) and (61) to fully describe the relation between strain rate, stress, temperature, grain size, and grain boundary thickness would demand the derivation of the precise dependence of $\langle \nu \rangle$ and σ_0 on these variables. However, the comparison with a large amount of experimental results indicates that this task is of minor utility because eventual variations of $\langle \nu \rangle$ and σ_0 are not observed under the physical conditions used in the experiments.

The previous discussion assumes an ideal situation, in which the grain boundary surfaces are planar with no defects. However, any step or hard second-phase particle intersecting a boundary may stabilize more the spatial distribution of trenches or change the period of the phenomenon, since it must be commensurate with a different distance, smaller than the grain size. As the occurrence of defects in the grain boundaries is statistically proportional to the grain size through a fixed constant, the linear relation between 2ℓ and d is maintained.

The constitutive equation (54) with the coefficient C_0 given by Eq. (61) and $\Omega^*=0$ has some formal resemblance with the boundary term of the equation given by Ashby and Verrall.[16] The theories behind them are quite different, indeed. Here, D_0 is not related to boundary diffusion, but to vacancy transport through crystalline matter. The exponential dependence of the strain rate on the flow stress and the constant Ω^*, absent in the work of Ashby and Verrall, are capital in the present approach, together with the factor $\langle\nu\rangle^2$, which accounts for the buckling degree of the grain boundaries.

The size of the constant Ω^* is what makes the difference between superplastic and nonsuperplastic materials. In effect, the strain rate increases exponentially with $\Omega^*\sigma$ and the mechanism for grain boundary sliding explained before will dominate over other possible deformation processes if Ω^* is large enough.

VI. GRAIN SHAPE ACCOMMODATION AND LOSS OF SUPERPLASTIC PROPERTIES

The theoretical approach to superplastic deformation put forward above gives all the credit to grain boundary sliding. However, two grains cannot slide without modifying continuously their irregular shapes to maintain contact over all their surfaces, at the atomic level, with other surrounding units. Therefore, it cannot be disregarded that grain boundary sliding is necessarily concurrent with the continuous deformation of all the crystallites involved in the process. One may adopt the point of view that the plastic flow of the material is caused primarily by the sliding of its crystallites and that the simultaneous grain deformation is an effect of that sliding. In this view, the issue is how the continuous shape accommodation of the grains affects the relative speed Δv between adjacent grains. Certainly, the accommodation of sliding grains involves shear forces that reduce the driving force causing the relative motion between these grains.

Consider a plane grain boundary surface, parallel to the $x'y'$ plane, that slides along the x' direction toward a triple junction. The surface of the crystal beyond the junction makes an angle ϕ with the $x'y'$ plane. To maintain the sliding speed Δv the crystal matter should undergo a continuous shear deformation of magnitude $\varepsilon_{z'x'}=\tan\phi$ at the junction. This deformation is produced by a shear force perpendicular to the $x'y'$ plane, induced by the grain shift. Hence a local shear stress field $\sigma^{\mathrm{ind}}_{z'x'}$, associated with the deformation shear force, arises as a consequence of the sliding. However, assuming quasiequilibrium where

$$\sigma^{\mathrm{ind}}_{z'x'}=\sigma^{\mathrm{ind}}_{x'z'}, \tag{63}$$

which means that a shear stress $\sigma^{\mathrm{ind}}_{x'z'}$, opposed to the shear stress $\sigma_{x'z'}$ originated by the external forces applied to the material, is induced in the $x'y'$ plane. Therefore, the sliding relative speed between the grains is now

$$\Delta v_{x'}=\mathcal{Q}(\sigma_{x'z'}-\sigma^{\mathrm{ind}}_{x'z'}) \tag{64}$$

instead of Eq. (37). Of course, sliding is possible only if $\sigma_{x'z'}>\sigma^{\mathrm{ind}}_{x'z'}$.

The relation between $\sigma^{\mathrm{ind}}_{x'z'}$ and $\sigma_{x'z'}$ is not simple because the mechanism of crystal deformation is not. However, one does not need to go into the details of the deformation processes to obtain what is important for our problem. Making the very natural assumption that the volume $d^2\Delta v_{x'}$ which is being deformed in $\varepsilon_{z'x'}=\tan\phi$ per unit time is proportional to the induced shear stress $\sigma^{\mathrm{ind}}_{z'x'}$ one can write

$$\sigma^{\mathrm{ind}}_{z'x'}=\Gamma\Delta v_{x'}. \tag{65}$$

Replacing this in Eq. (64) and solving for $\Delta v_{x'}$ obtains

$$\Delta v_{x'}=\frac{\mathcal{Q}}{1+\Gamma\mathcal{Q}}\sigma_{x'z'}. \tag{66}$$

In this way the general form of Eq. (37) is recovered.

However, while the coefficient Γ is expected to be almost independent of temperature and stress, $\mathcal{Q}$ varies exponentially with these two variables, as given by Eqs. (38) and (50). Therefore, one can expect that $\Gamma\mathcal{Q}\approx 1$ only under very special conditions of temperature and stress, and that the most common situations are

$$\Delta v_{i'}=\begin{cases}\mathcal{Q}\,\sigma_{i'z'}, & \mathcal{Q}\ll 1/\Gamma,\\ (1/\Gamma)\sigma_{i'z'}, & \mathcal{Q}\gg 1/\Gamma,\end{cases}\quad i'=x',y'. \tag{67}$$

The simple equation (67) expresses a very important result. In the first case, grain boundary sliding dominates the plastic flow of the polycrystal and grain shape accommodation has a minor effect. As $\mathcal{Q}$ increases rapidly with temperature and stress, the first case occurs for moderate enough values of these variables. For higher temperatures or stresses the system may enter the second case, in which the reluctance of the grains to be deformed imposes a limit to the plastic strain rate. In this second situation of a high plastic strain rate or high temperature, the equations of the previous section cease to be valid. It follows a very neat explanation to why the high ductility associated with superplasticity is reduced for temperatures higher than the ideal. Also a too fine-grained size d may increase $\mathcal{Q}$ to force the system into the second regime, which is presumably nonsuperplastic. Therefore, in the present theory the occurrence of superplasticity demands that $\mathcal{Q}$ be high enough to ensure that the mechanism explained above contributes the most to the strain rate, but not so high that $\Gamma\mathcal{Q}\gg 1$, in which case the system would enter the second regime of deformation.

One can conclude as well that, when not dominant, grain shape accommodation does not affect significantly the constitutive equation relating stress, strain rate, temperature, grain size, and grain boundary thickness derived previously.

VII. COMPARISON WITH EXPERIMENT

For $\sigma_0=0$, Eq. (54) is formally identical to the result obtained in Ref. 20. Apart from some trivial constants in the definition of the coefficient C_0 and the implicit dependence of ℓ on d, the only difference is the factor $1/3$ of Ω^* in the argument of the exponential function. It is due only to the definition of σ, which in that previous paper was simply the sum of the principal stresses. Figure 1of Ref. 20 shows

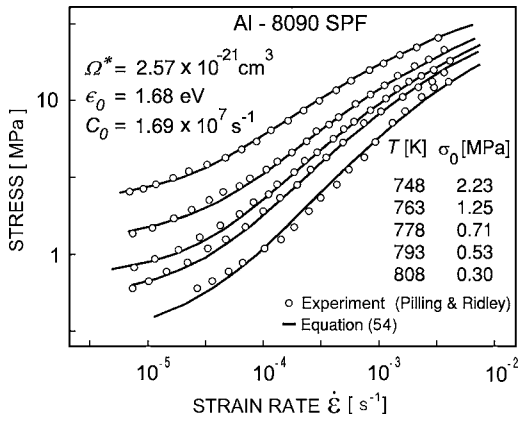

FIG. 5. Plot of the experimental results of Ref. 42 for the alloy Al-8090 SPF at the five temperatures indicated in the graph. The solid lines represent Eq. (54) with the constants Ω^*, ϵ_0, and C_0 appearing in the inset. Small variations of C_0 around the shown value were accomplished in order to optimize the fit for each temperature. The other two parameters are the same in the five curves. The values of σ_0 were chosen to optimize the fit at $\dot{\varepsilon} \leqslant 5 \times 10^{-5}$ s^{-1}.

how well Eq. (54) with $\sigma_0=0$ can reproduce the experimental data of Hamilton, Bampton, and Paton[41] for the aluminum alloy Al-7475 at four temperatures in the superplastic regime.

Figure 5 exhibits the uniaxial tensile stresses $\sigma_z=3\sigma$ applied to samples of Al-8090 SPF, another superplastic aluminum-based alloy, very popular in airplane construction, to achieve constant stress rates $\dot{\varepsilon}$ at the five temperatures displayed in the inset. The solid curves represent the results given by Eq. (54) and the experimental points are due to Pilling and Ridley.[42] The magnitudes of the constants Ω^*, ϵ_0, and C_0 are also shown in the figure. While the former two constants are the same for all curves, the value shown for C_0 is only an average because a small dispersion was found for this magnitude in order to optimize the fit of the four curves independently. The values for the temperature dependent threshold stress σ_0, listed with the temperatures, were chosen to improve the fits at $\dot{\varepsilon} \leqslant 5 \times 10^{-5}$ s^{-1}.

Figure 6 shows experimental results of Hamilton *et al.*, who tested for superplastic deformation four classes of samples of Al-7475 that differ only in grain size.[41] In addition to the scans for several temperatures performed with one of these materials, displayed in Fig. 1 of Ref. 20, the procedure was conducted for the three other classes of samples at the unique temperature $T=789$ K. The grain shape was in all cases rather elongated, having short transverse dimensions d_{ST} of 6.4, 7.8, 8.5, and 10.7 μm. The corresponding longitudinal dimensions d_L were close to twice d_{ST} in the four classes of samples. Two tests with samples whose grains were extremely asymmetrical, with d_L as large as 69.4 and 156.3 μm, were also carried out, but gave poor ductility, no superplastic behavior, and therefore are disregarded here. The alloy Al-7475 is specially suited for testing theory because it has a particularly stable grain size under changing conditions of temperature, deformation, and deformation rate. The experiment of Hamilton, Bampton, and Paton is also particularly accurate and complete, and scans a wide range of temperatures.

Figure 6 exhibits the experimental data referred to in the previous paragraph. The four plots are identified by the mean grain size d. The solid lines represent Eq. (54) with the same values of the constants Ω^* and ϵ_0 obtained from the fit of the temperature-dependent data accomplished in Ref. 20. Again, $\sigma_0=0$. Hence the only adjustable parameter for the fit of the four sets of data in Fig. 6 is C_0.

Figure 7 exhibits a logarithmic plot of the values of C_0 obtained from the best fit to the experimental points of Fig. 6 as a function of the mean grain size d. The data arrange very close to the straight line

$$\log_{10} C_0 = -3 \log_{10} d + 11.91, \tag{68}$$

where the units are those of the graph. The highly accurate d^{-3} dependence of C_0 is clearly demonstrated by Fig. 7.

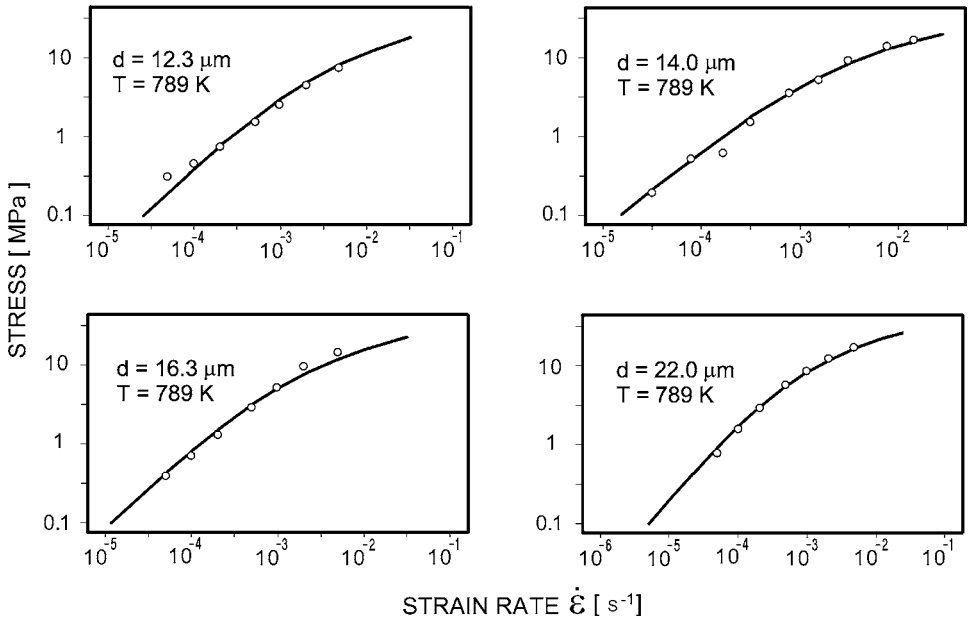

FIG. 6. The data of Hamilton, Bampton, and Paton (Ref. 41) for Al-7475 at $T=789$ K and samples having four different grain sizes d. The solid lines represent Eq. (54) with Ω^* and ε_0 obtained in Ref. 20. C_0 was chosen to attain the best fit between the theoretical curve and the data for each grain size (notice that the definition of Ω^* in Ref. 20 differs from the one given here by a factor 1/3).

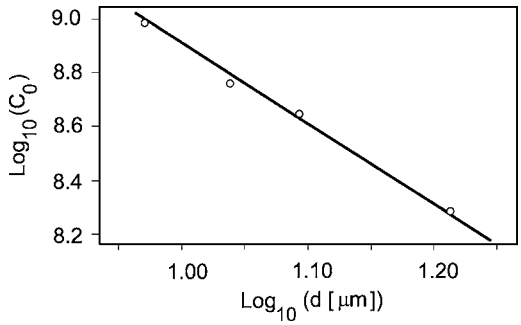

FIG. 7. The values of C_0 that produce the four curves displayed in Fig. 6 are shown in a graph of $\log_{10} C_0$ vs $\log_{10} d$. The four points lie very close to a straight line with slope −3, which shows the d^{-3} dependence of C_0 on the grain size.

Figure 8 shows another example of application, this time in the commercial superplastic alloy Ti-6Al-4V, which is probably the titanium superplastic alloy most used in airplane design. The circles represent the data taken by Cope[43] and Cope *et al.*[44,45] at the six temperatures appearing in the figure. Another inset exhibits the magnitude of the constants Ω^*, ϵ_0, and C_0 that, inserted into Eq. (54) together with the corresponding temperature, give the solid lines. The six curves were obtained with exactly the same set of parameters and no dispersion was found for them. The agreement between theory and experiment is striking, and perhaps better for titanium than aluminum, because C_0 does not exhibit any random variations with T, as was the case for the latter material. Small values of σ_0 were used to improve the fits in the region below $\dot{\varepsilon}=5\times10^{-5}$ s^{-1}.

Replacing in Eq. (59) $C_0=3.52\times10^4$ s^{-1}, which is the value obtained from the fit to the experimental results for titanium, the mean grain size $d=2.28$ μm (the grain size varied with temperature between 1.5 and 4.0 μm), $d_1=3\times10^{-7}$ cm, and D_0 from tables, one can estimate $\langle\nu\rangle^2$ and, inserting the result in Eq. (62), check whether a reasonable range for the stresses is obtained. Unfortunately, only a very rough estimation can be done at present because the value of the preexponential factor D_0 of the diffusion coefficient (48), appearing in expression (58), is rather uncertain. Measurements of Ti autodiffusion give values for D_0 as different as 3.58×10^{-4} cm^2 s^{-1} (Ref. 46) and 1.6×10^{-3} cm^2 s^{-1} (Ref. 47). The corresponding activation energies ϵ_a in these two experiments do not differ remarkably (31.2 and 35 [K cal/model], respectively). The precise measurement of D_0 is quite difficult because, as the exponential factor in expression (51) varies rapidly with ϵ_a, a relatively small error in the activation energy may produce a large variation of D_0 in order to fit the experimental data. Additionally, in our case we are considering the diffusion of vacancies in paths close to the grain boundary, which is not the normal condition. With the previous remarks one obtains

$$\langle\nu\rangle^2=\begin{cases}1413; & D_0=3.58\times10^{-4}\ \text{cm}^2\ \text{s}^{-1},\\ 316, & D_0=1.6\times10^{-3}\ \text{cm}^2\ \text{s}^{-1},\end{cases}\tag{69}$$

which correspond to an average of 18 and 9 trenches per sliding grain facet, respectively. Inserting $E=1.16\times10^{11}$ Pa (Ref. 48) relation (62) becomes

$$31\ \text{MPa}\leqslant\tau\leqslant125\ \text{MPa},\quad D_0=3.58\times10^{-4}\ \text{cm}^2\ \text{s}^{-1},$$

$$7\ \text{MPa}\leqslant\tau\leqslant28\ \text{MPa},\quad D_0=1.6\times10^{-3}\ \text{cm}^2\ \text{s}^{-1}.\tag{70}$$

In both situations the range of variation for the shear stress falls in the range of the stress applied to the sample, which proves the consistency of the theory.

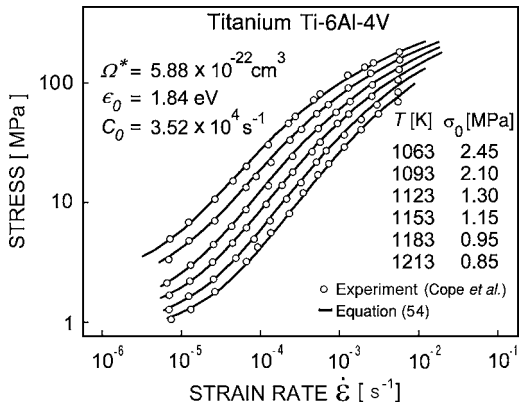

FIG. 8. Plot of the experimental results of Refs. 43–45 for the titanium alloy Ti-6Al-4V at the six temperatures indicated in the inset. The solid lines represent Eq. (54) with the constants Ω^*, ϵ_0, and C_0 appearing in the left side of the graph. The six curves use the same constants, and no adjustment of C_0 was done to improve the fit at different temperatures. A small threshold stress σ_0 was introduced, which improves the concordance with the experiment below $\dot{\varepsilon}=5\times10^{-5}$ s^{-1}.

Equation (54) reproduces with great accuracy the deformation properties of superplastic alloys over the whole range of strain rate, stress, and temperature in which superplasticity is observed. From a practical point of view, it permits the classification of superplastic materials by three constants and is certainly a much better constitutive equation than the power law usually utilized.

In the scheme put forward here, the physical origin of the phenomenon is the mechanical instability of grain boundaries subjected to overcritical stresses, which induces strong stress fields that vary rapidly in the subgrain scale. These stress gradients, in turn, affect the thermodynamical equilibrium between the grain boundaries and the adjacent grains. Two kinds of grain boundary mechanical instabilities were treated in Sec. III, but in particular Sec. III B. The effect explained in Sec. III C was discussed before, in Ref. 20. Formally, the only difference occurs in the coefficient C_0 and in its dependence on the grain size d. In general, other sources of strongly varying stress fields in the grain scale may be possible, but their formal consequences should affect only the coefficient C_0 of Eq. (54).

ACKNOWLEDGMENT

This work was partially supported by Fondecyt Grant 1020091.

*Electronic address: mlagos@macul.ciencias.uchile.cl

[1] E. D. Weisert and G. W. Stacher, in *Superplastic Forming in Structural Alloys*, edited by N. E. Paton and C. H. Hamilton (The Metallurgical Society of AIME, Warrendale, PA, 1982).
[2] J. Pilling and N. Ridley, *Superplasticity in crystalline solids* (The Institute of Metals, Camelot, Southampton, UK, 1989).
[3] T. G. Nieh, J. Wadsworth, and O. D. Sherby, *Superplasticity in Metals and Ceramics* (Cambrige University Press, Cambridge, UK, 1997).
[4] Y. Nakatani, T. Ohnishi, and K. Higashi, Jpn. Inst. Met. **48**, 113 (1984).
[5] O. Sherby and J. Wadsworth, Prog. Mater. Sci. **33**, 169 (1989).
[6] A. Ball and M. M. Hutchinson, Met. Sci. J. **3**, 1 (1969).
[7] T. G. Langdon, Philos. Mag. A **22**, 689 (1970).
[8] A. K. Mukherjee, Mater. Sci. Eng. **8**, 83 (1971).
[9] H. W. Hayden, S. Floreen, and P. D. Googall, Metall. Trans. A **3**, 833 (1972).
[10] R. C. Gifkins, Metall. Trans. A **7**, 1225 (1976).
[11] H. G. Gittus, ASME J. Eng. Mater. Technol. **99**, 244 (1977).
[12] A. Arieli and A. K. Mukherjee, Mater. Sci. Eng. **45**, 61 (1980).
[13] O. D. Sherby and J. Wadsworth, in *Deformation Processing and Structure*, edited by G. Krauss (ASM, Metal Park, OH, 1984).
[14] O. K. Kaibyshev, R. Z. Valiev, and A. K. Emaletdinov, Phys. Status Solidi A **90**, 197 (1985).
[15] H. Fukuyo, H. C. Tsai, T. Oyama, and O. D. Sherby, ISIJ Int. **31**, 76 (1991).
[16] M. F. Ashby and R. A. Verrall, Acta Metall. **21**, 149 (1973).
[17] K. A. Padmanabhan, Mater. Sci. Eng. **40**, 285 (1979).
[18] J. S. Vetrano, E. P. Simonen, and S. M. Bruemmer, Acta Mater. **47**, 4125 (1999).
[19] J. S. Vetrano, C. H. Henager, and E. P. Simonen, in *Superplasticity—Current Status and Future Potential*, edited by P. B. Berbon, M. Z. Berbon, T. Sakuma, and T. Langdon (Materials Research Society, Warrendale, PA, 2000).
[20] M. Lagos, Phys. Rev. Lett. **85**, 2332 (2000).
[21] K. Murali and N. Chandra, Acta Metall. Mater. **43**, 1783 (1995).
[22] M. Lagos, in *Proceedings of the Fourth Pacific International Conference on Advanced Materials and Processing*, edited by S. Hanada, Z. Zhong, S. W. Nam, and R. N. Wright (The Japan Institute of Metals, Sendai, Japan, 2001).
[23] J. M. Burgers, Proc. Phys. Soc. London **52**, 23 (1940).
[24] J. M. Burgers, Proc. K. Ned. Akad. Wet. **42**, 293 (1939).
[25] W. T. Read and W. Shockley, Phys. Rev. **78**, 275 (1950).
[26] T. Meyer and H. von Känel, Phys. Rev. Lett. **78**, 3133 (1997).
[27] M. Lagos and H. Duque, Solid State Commun. **99**, 329 (1996).
[28] M. Lagos and H. Duque, Solid State Commun. **107**, 311 (1998).
[29] M. Lagos and H. Duque, Int. J. Plast. **17**, 369 (2001).
[30] P. Bellon and R. S. Averback, Phys. Rev. Lett. **74**, 1819 (1995).
[31] D. J. Srolovitz, Acta Metall. **37**, 621 (1989).
[32] J. Müller and M. Grant, Phys. Rev. Lett. **82**, 1736 (1999).
[33] M. A. Grinfeld, Dokl. Akad. Nauk SSSR **265**, 836 (1982); Sov. Phys. Dokl. **31**, 831 (1986); Europhys. Lett. **22**, 723 (1993).
[34] D. R. M. Williams, Phys. Rev. Lett. **75**, 453 (1995).
[35] F. Y. Génin, J. Appl. Phys. **77**, 5130 (1995).
[36] D. E. Jones, J. P. Pelz, Y. Hong, E. Bauer, and I. S. T. Tsong, Phys. Rev. Lett. **77**, 330 (1996).
[37] D. E. Jesson, K. M. Chen, S. J. Pennycook, T. Thundat, and R. J. Warmack, Phys. Rev. Lett. **77**, 1330 (1996).
[38] P. C. Searson, R. Li, and K. Sieradzki, Phys. Rev. Lett. **74**, 1395 (1995).
[39] R. Q. Hwang, J. C. Hamilton, J. L. Stevens, and S. M. Foiles, Phys. Rev. Lett. **75**, 4242 (1995).
[40] W. Barvosa-Carter, M. J. Aziz, L. J. Gray, and T. Kaplan, Phys. Rev. Lett. **81**, 1445 (1998).
[41] C. H. Hamilton, C. C. Bampton, and N. E. Paton, in *Superplastic Forming in Structural Alloys*, edited by N. E. Paton and C. H. Hamilton (The Metallurgical Society of AIME, Warrendale, PA, 1982).
[42] J. Pilling and N. Ridley, in *Aluminium Technology '86*, edited by T. Sheppard (Institute of Metals, London, UK, 1986).
[43] M. T. Cope, M.Sci. thesis, Victoria University of Manchester, 1982.
[44] M. T. Cope and N. Ridley, Mater. Sci. Technol. **2**, 140 (1986).
[45] M. T. Cope, D. R. Evetts, and N. Ridley, J. Mater. Sci. **21**, 4003 (1986).
[46] J. F. Murdock, T. S. Lundy, and E. E. Stanbury, Acta Metall. **12**, 1033 (1964).
[47] Y. Adda and J. Philibert, *La difusion dans les solides* (Presses Universitaires de France, Paris, 1966).
[48] *American Institute of Physics Handbook*, 3rd ed., edited by D. E. Gray (McGraw-Hill, New York, 1972).